

# Crystal structure of the class D $\beta$ -lactamase OXA-10

Mark Paetzel<sup>1</sup>, Franck Danel<sup>2</sup>, Liza de Castro<sup>1</sup>, Steven C. Mosimann<sup>1</sup>, Malcolm G.P. Page<sup>2</sup> and Natalie C.J. Strynadka<sup>1</sup>

We report the crystal structure of a class D  $\beta$ -lactamase, the broad spectrum enzyme OXA-10 from *Pseudomonas aeruginosa* at 2.0 Å resolution. There are significant differences between the overall fold observed in this structure and those of the evolutionarily related class A and class C  $\beta$ -lactamases. Furthermore, the structure suggests the unique, cation mediated formation of a homodimer. Kinetic and hydrodynamic data shows that the dimer is a relevant species in solution and is the more active form of the enzyme. Comparison of the molecular details of the active sites of the class A and class C enzymes with the OXA-10 structure reveals that there is no counterpart in OXA-10 to the residues proposed to act as general bases in either of these enzymes (Glu 166 and Tyr 150, respectively). Our structures of the native and chloride inhibited forms of OXA-10 suggest that the class D enzymes have evolved a distinct catalytic mechanism for  $\beta$ -lactam hydrolysis. Clinical variants of OXA-10 are also discussed in light of the structure.

$\beta$ -Lactamases comprise the most widespread means by which bacteria resist  $\beta$ -lactam antibiotics, including penicillins, cephalosporins, and monobactams<sup>1</sup>. These enzymes can be categorized into four classes (termed A through D) based on their sequence similarities and substrate profiles<sup>2</sup>. Class A, C and D enzymes are serine hydrolases while the class B  $\beta$ -lactamases are metalloenzymes<sup>3,4</sup>. The serine  $\beta$ -lactamases and the D-Ala-D-Ala transpeptidases (DD-transpeptidases), which are responsible for the biosynthesis of the bacterial cell wall and are targets of the  $\beta$ -lactam antibiotics, are thought to have a common evolutionary history<sup>5,6</sup>. Despite varying sizes and limited overall sequence identities, comparison of the sequences and crystallographic structures of the class A, class C and the DD-transpeptidases has identified three common motifs (referred to as the 'active site elements'; Table 1). The corresponding elements in class D enzymes have been identified only by sequence alignments (sequence identities between the class D and the class A and C enzymes are on average 16%<sup>7</sup>), as no structural work has been available for the class D enzymes. Increasing numbers of class D enzymes are being found in the clinic, primarily located on plasmids or integrons. This potential for wide dispersal, taken together with the broad substrate specificity and lack of

clinically useful inhibitors, underlines the importance of investigating the molecular details of this fourth class of  $\beta$ -lactamase<sup>7-9</sup>.

## Overall fold of OXA-10

The 247 amino acids of OXA-10 fold into an  $\alpha/\beta$  structure of dimensions 43 Å × 50 Å × 47 Å (Fig. 1a,b). The structure can be

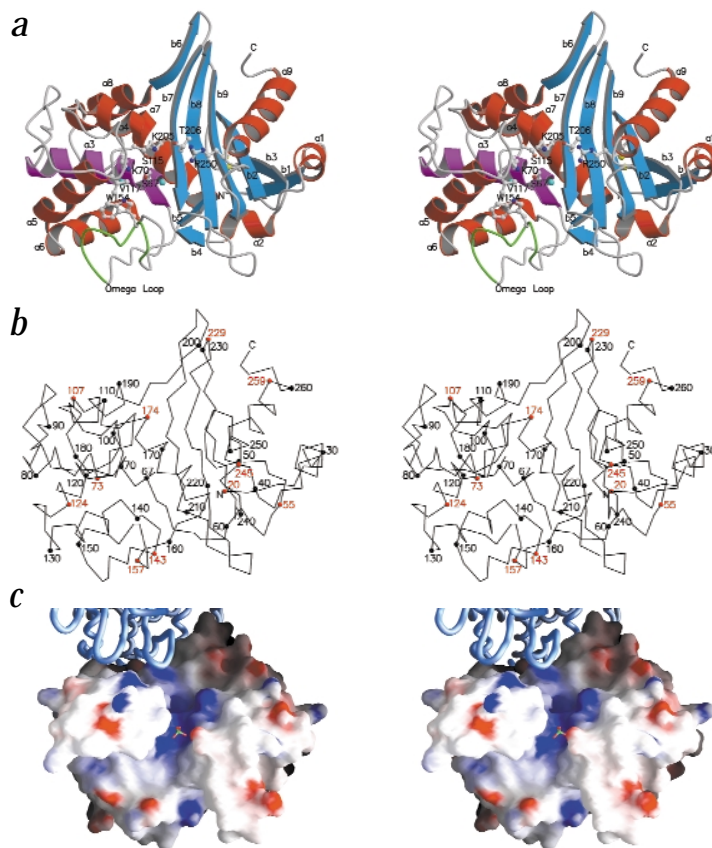


**Fig. 1** The protein fold of the class D  $\beta$ -lactamase OXA-10. **a**, Stereo view of a ribbon<sup>43</sup> representation of one monomer of OXA-10. The side chains of selected residues within the active site are shown in ball and stick representation. The helix containing the Ser 67 nucleophile is shown in purple. The omega loop common to all serine  $\beta$ -lactamases and DD-peptidases is shown in green. **b**, Stereo view of a C $\alpha$  trace<sup>43</sup> in the same orientation as (a), with sequential numbering of every 10<sup>th</sup> residue. Residues that are mutated in clinical variants of OXA-10 are shown with a red sphere at their C $\alpha$  position and labeled in red. **c**, Stereo view of a GRASP<sup>44</sup> generated electrostatic surface of OXA-10. Areas of negative charge are shown in red, and areas of positive charge in blue. The second molecule of the observed OXA-10 dimer is shown as a C $\alpha$  backbone representation (blue worm).

<sup>1</sup>Department of Biochemistry and Molecular Biology, University of British Columbia, 2146 Health Sciences Mall, Vancouver, British Columbia, V6T 1Z3, Canada.

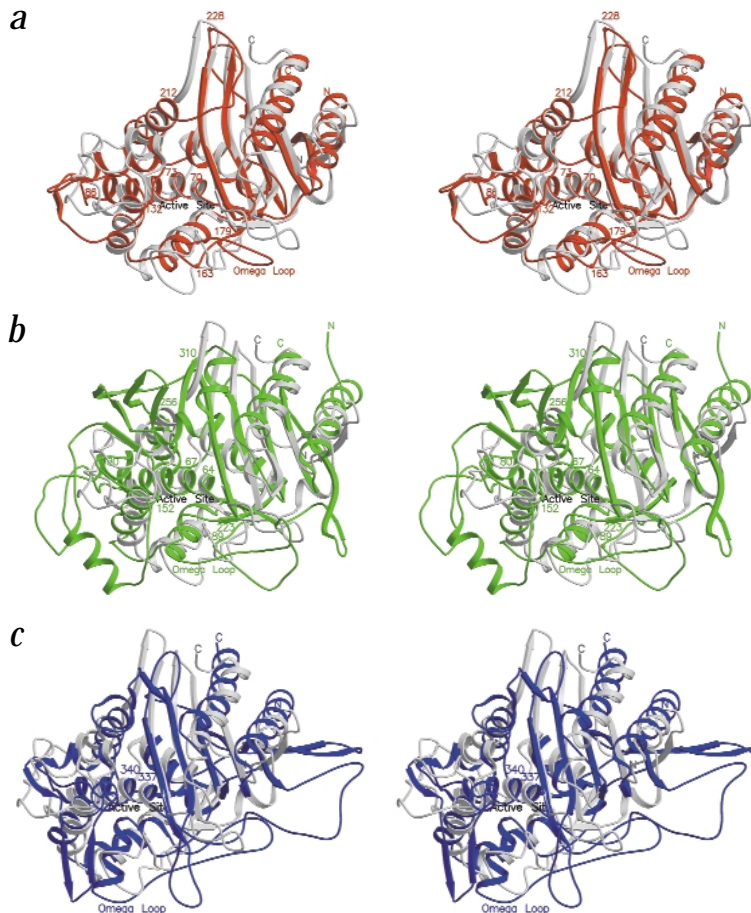
<sup>2</sup>F. Hoffman-La Roche Ltd., Pharma Division, Preclinical Research, CH-4070 Basel, Switzerland.

Correspondence and requests for materials should be addressed to N.C.J.S. email: [natalie@byron.biochem.ubc.ca](mailto:natalie@byron.biochem.ubc.ca)



# articles

**Fig. 3** Superpositions of the overall fold of class D OXA-10 with related enzymes. **a**, Stereo view of the superposition of OXA-10 (gray ribbon<sup>43</sup>) with a representative class A  $\beta$ -lactamase (*E. coli* TEM-1<sup>10,11</sup>, red ribbon, PDB accession code 1FQG). **b**, Stereo view of the superposition with a representative class C  $\beta$ -lactamase (*C. freundii*<sup>2</sup>, green ribbon, PDB accession code 1FR6). **c**, Stereo view of the superposition with the transpeptidase domain of PBP2x (*S. pneumoniae*<sup>6</sup>, blue ribbon, PDB accession code 1QME).



acter in OXA-10 include Met 99, Trp102, Val 117, Leu 155, Phe 208 and Leu 247 (Fig. 2). Collectively these features may serve to accommodate a broad range of side groups in the  $\beta$ -lactam substrates as has been suggested for the metallo- $\beta$ -lactamase family<sup>4</sup> and may explain earlier findings that class D enzymes are inhibited by bulky hydrophobic dyes<sup>13</sup>.

Superposition of OXA-10 with DD-transpeptidase PBP2x from *Streptococcus pneumoniae* (Fig. 3c) reveals structural similarity between them as predicted from earlier sequence alignment studies<sup>2,14</sup> (the r.m.s. deviation is 2.3 Å for 183 C $\alpha$  atoms). This indicates that the class D enzymes have more backbone positions in common with the cell wall transpeptidase than with either the class A or class C  $\beta$ -lactamases.

## Dimerization of OXA-10

The two similar molecules of the OXA-10 asymmetric unit (r.m.s. deviation of 0.4 Å for 243 C $\alpha$  atoms) are related by  $\sim$ two-fold symmetry and are intimately associated, with 1,130 Å<sup>2</sup> of surface area buried per monomer (Fig. 4a). Several electrostatic (including two salt bridges) and 10 direct hydrogen bonding interactions stabilize the dimer. The interface centers about residues 181–193 (a8) and 194–198 (b6). The two b6 strands run antiparallel to each other and interact *via* hydrophobic (side chain of Ala 196) and water mediated interactions. Several hydrophobic interactions also arise from symmetrically disposed residues within a8 in each monomer (Leu 186, Ile 187 and Val 193). Our structure identifies two cobalt atoms bound at the dimer interface coordinated by the carboxylate oxygen of Glu 190 in one monomer and the carboxylate oxygens from Glu 227 and imidazole nitrogen from His 203 in the second monomer (Fig. 4b). Two waters complete the octahedral coordination. The ligand distances in each site range from 2.1 to 2.3 Å, typical of zinc and cobalt binding sites<sup>15</sup>. Several of the residues at the interface, including Glu 190, His 203 and Glu 227, are conserved among several of the class D enzymes (OXA-5, 7, 10, 11, 13, 14, 16, 17 and 19; Fig 2). Other species (OXA-2, 3, 15, 20 and 21) contain conservative substitutions at the interface as well as the substitutions E190D and H203R, suggesting that a salt bridge may replace the cation site in these species (Dale and Smith<sup>16</sup> provided earlier evidence for the formation of OXA-2 dimers in solution). It is possible that in some species the significant hydrophobic and hydrogen bonding interactions are sufficient to induce dimerization in the absence of additional cation binding sites.

Kinetic and hydrodynamic evidence supports our structural data, with maximal activity observed for the dimeric form of OXA-10 and occurring in the presence of cations (Table 2). Dimer formation and enzyme activity is promoted optimally by zinc, copper and cadmium ions, although nickel, manganese and cobalt ions also mediate the effect to a lesser degree. No significant increase in activity was observed for calcium, magnesium, sodium or potassium.

The calculated molecular weight (MW) of OXA-10 based on sequence is 27,550 Da. Analytical ultracentrifugation shows that OXA-10 has a MW corresponding to the dimeric form (55,100 Da) at concentrations of enzyme between 1 and 20  $\mu$ M. At concentrations of 0.01  $\mu$ M, the estimated MW was 29 kDa (monomer). However, in the presence of 0.5 mM cadmium, copper or zinc, the apparent MW at the lower OXA-10 concentration (0.01  $\mu$ M) increased to the dimeric 53 kDa value (Table 2).

The enzyme activity assays were performed at a low concentration of enzyme (0.025  $\mu$ M). Under these conditions, OXA-10  $\beta$ -lactamase would exist primarily in a monomeric form in the absence of cations. An excellent correlation was observed between the increase in activity against nitrocefin and the cation mediated formation of dimers, showing that the enzyme is more active in the dimeric form. Both OXA-10 and OXA-14 have been shown to have complex biphasic kinetics with some substrates<sup>17</sup>, which may now be explained by the conversion of the dimeric form of the enzyme to a less active monomeric form during the course of the assay. A  $\beta$ -turn between b6 and b7 in one monomer lies on the periphery of the binding site of the adjacent monomer (Fig. 1c). Although unlikely to play a catalytic role (as it is >18 Å away), it could affect substrate binding and, in combination with conformational or stability differences between the monomeric and dimeric forms, may explain the differences in the kinetic profiles for various substrates of the class D enzymes<sup>7,17</sup>.

## The class D active site elements

Class D enzymes contain three active site elements. In OXA-10, the active site centers about the conserved residues of element 1

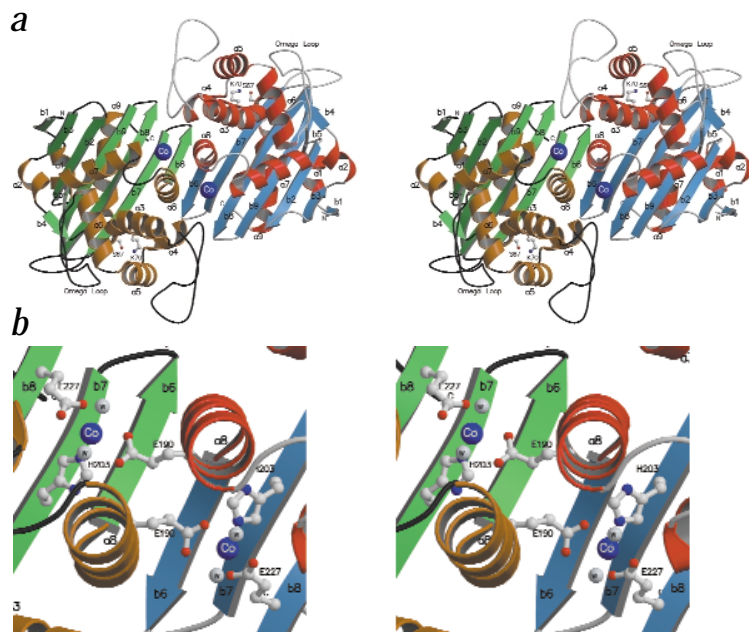


**Fig. 4** The OXA-10 homodimer. **a**, Stereo view of a ribbon representation<sup>43</sup> of the observed OXA-10 homodimer. One monomer is in green and gold, the other in blue and red. The two cobalt atoms that lie at the dimer interface are shown in dark blue. The active site residues Ser 67 and Lys 70 are shown in ball and stick representation. It should be noted that the active site of each monomer lies on the same face of the dimer and are ~40 Å apart. **b**, Stereo view of the coordination of the cobalt atoms (blue) by the coordinating ligands Glu 227 and His 203 within one monomer and Glu 190 within the second monomer. Two ordered waters (small spheres) complete the approximate octahedral coordination of each cobalt. The refined temperature factor of each cobalt atom is 19.5 Å<sup>2</sup>.

(Ser 67-X-X-Lys 70 where X represents any amino acid), which lie on the N-terminal end of the 3<sub>10</sub>-helix a3. The side chains of Ser 67 and Lys 70 form a strong hydrogen bond with each other (2.9 Å; Figs 1a, 5a,b). Lys 70 makes a second hydrogen bond to a buried and ordered water (WAT2; Fig. 5a,b) that is also coordinated to the side chain nitrogen of the conserved Trp 154 that protrudes from the omega loop. Lys 70 is fully buried and is in an unusually hydrophobic environment, forming van der Waals contacts with Ile 112, Ser 115, Val 117, and Phe 120 (Figs 2, 5a). The only charged amino acid within 10 Å of Lys 70 is the conserved Lys 205 (5.3 Å from Nζ to Nζ).

Ending controversy from earlier sequence analysis studies<sup>1,14</sup>, our structure shows that the second active site element in the class D enzymes is the conserved motif Ser 115-X-Val 117 (Table 1, Figs 1a, 2, 5a,b). Ser 115 and Val 117 lie on a linker between a4 and a5 (Figs 1a, 5a,b). The side chain Oγ of Ser 115 forms a hydrogen bond to Lys 205 (2.9 Å) and is within 3.5 Å of the Nζ and Oγ side chain atoms of Ser 67 and Lys 70, respectively (Fig. 5a). The presence of a nonpolar side chain (Val 117) within element 2 is unique to the class D enzymes. In the class A and C β-lactamases, this site contains an Asn residue that forms hydrogen bonds with the carbonyl oxygen of the substrate amide (Table 1, Fig. 5c,d), and the Nζ of Lys 70 in element 1 (refs 10,12,18,19). The smaller, nonpolar side chain of Val 117 may contribute to the broader substrate specificity within the class D enzymes, providing room for bulkier side groups (for example the isoxazolyl moiety of oxacillins) and interacting *via* hydrophobic rather than hydrogen bonding interactions. The group of penicillin sensor proteins that regulate β-lactamase and β-lactam-resistant transpeptidase expression in Gram-positive bacteria, and in which the deacylation activity is apparently absent<sup>20</sup>, contain similar active site elements as the class D β-lactamases. The only substitution within them is the presence of a polar residue (Thr/Asn) instead of Val 117 (Fig. 2).

The third active site element in the class D enzymes comprises Lys 205, Thr 206 and Gly 207 (Table 1, Fig. 5a). The analogous element in the class A and class C enzymes has been shown to be important for the binding of the carboxylate of the

β-lactam antibiotic<sup>5,10,12,19</sup> (Fig. 5c,d). That element 3 residues in OXA-10 have a similar role is supported by the observation of a strongly bound sulfate ion in the active site. Superposition of the active site residues in OXA-10 with those from the acyl-enzyme intermediate of class A TEM-1 (ref. 10) (Fig. 5c) indicates that the atoms of the benzylpenicillin carboxylate overlap with the sulfate ion position. Unexpectedly, the side chain of Arg 250 in OXA-10 protrudes from a9 to lie proximal to the element 3 residues and is positioned to contribute to the binding of the substrate carboxylate (Figs 1a, 5a). A similar role is observed for an Arg side chain in the class A enzymes<sup>21</sup> (Arg 244; Fig. 5c), despite it having a different position in the primary and tertiary structures.

#### Clinical variants of OXA-10

Several point mutations of OXA-10 that have varying substrate specificities have been isolated in the clinic<sup>7</sup>. OXA-11, 14, 16 and

**Table 2** The effect of cationic metals on the catalytic activity and apparent molecular weight of OXA-10 β-lactamase<sup>1</sup>

	Activity (%) <sup>2</sup>	Apparent molecular weight (%) <sup>3</sup>	
		29 kDa (monomer)	53 kDa (dimer)
CaCl <sub>2</sub>	105	80	20
CdCl <sub>2</sub>	165	0	100
CoCl <sub>2</sub>	142	30	70
CuSO <sub>4</sub>	175	0	100
MgSO <sub>4</sub>	105	100	0
MnCl <sub>2</sub>	112	85	15
NiCl <sub>2</sub>	130	70	30
ZnCl <sub>2</sub>	165	0	100
KCl	102 (73) <sup>4</sup>	100 (100) <sup>4</sup>	0 (0) <sup>4</sup>
EDTA	104	100	0
–	100	100	0

<sup>1</sup>The concentration of the metals was 0.5 mM unless otherwise specified and all assays were performed in 0.1 M Tris/H<sub>2</sub>SO<sub>4</sub> pH 7.0, 0.3 M K<sub>2</sub>SO<sub>4</sub>. The standard uncertainty is ±10% of the indicated value.

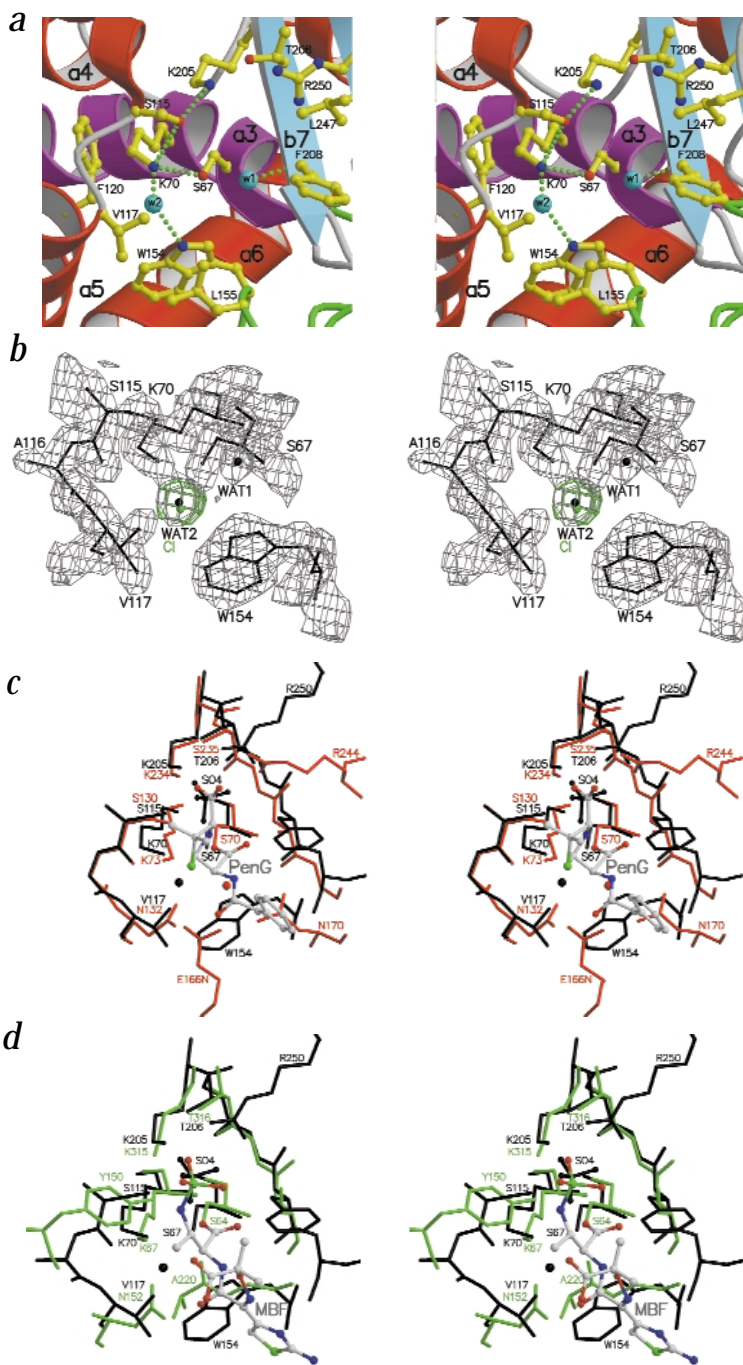
<sup>2</sup>Buffer without metals taken as 100%.

<sup>3</sup>As measured by size exclusion chromatography and ultracentrifugation (see methods). At an enzyme concentration of 0.01 μM in 0.1 M Tris/H<sub>2</sub>SO<sub>4</sub> pH 7.0 with 0.3 M K<sub>2</sub>SO<sub>4</sub> the apparent MW was 29 kDa (monomer), with 0% of the enzyme having a MW of 53 kDa (dimer). The observed cation mediated increase of MW was not due to an increase in the concentration of counter ions (sulfate or chloride) as sulfate was present in the buffer (0.3 M) to eliminate any interaction between the protein and column. The addition of a chloride counter ion at 5 or 50 mM did not have any effect on the apparent MW of the enzyme.

<sup>4</sup>Concentration at 5 mM KCl. NaCl had a similar effect.

## articles

**Fig. 5** The active site of OXA-10. **a**, Stereo view of a ball and stick representation<sup>43</sup> of the active site residues in OXA-10. Selected water molecules are shown as cyan spheres. Hydrogen bonds are shown as dotted green lines. For clarity, the sulfate ion observed in our structure is removed in this view. **b**, Stereo view of the final refined  $2F_o - F_c$  electron density ( $1.5 \sigma$ ) around key active site residues and water molecules in OXA-10  $\beta$ -lactamase.  $2F_o - F_c$  electron density ( $1.5 \sigma$ ) for a refined chloride ion in data obtained from crystals grown in 100 mM NaCl is shown in green (refined temperature factor =  $16 \text{ \AA}^2$ ). It is acknowledged that the position of the water in the native structure may also be partially occupied by chloride given the presence of 10 mM  $\text{CoCl}_2$  in the crystallization solution. Our refinement statistics suggest that it is primarily a water molecule. **c**, Stereo view of a stick representation of the superposition of the active site of OXA-10 (black) with the class A *E. coli* TEM-1-penicillin G (PenG) acyl-enzyme complex (red)<sup>10</sup>. The PenG substrate is shown in light gray ball and stick representation. A deacylation deficient mutation on the omega loop of TEM-1, Glu166Asn, was used to trap the acyl-enzyme. The proposed deacylating water of TEM-1 is shown as a red sphere. **d**, Stereo view of the superposition of the active site of OXA-10 (black) with the class C *C. freundii*-azetrenam (MBF) acyl-enzyme complex (green)<sup>12</sup>. The monobactam MBF is shown in light grey ball and stick representation.



17 are natural mutants of OXA-10  $\beta$ -lactamase that confer resistance to an extended spectrum of cephalosporins<sup>7</sup>. These mutations can be mapped onto the OXA-10 structure. We find that most of the mutations lie not within, but adjacent to the active site elements and are likely to exert their effects indirectly by altering the positions of the adjacent active site residues (Fig. 1b). For example, OXA-11 contains two substitutions (N143S and G157D) relative to OXA-10. Asn 143 is part of the Tyr-Gly-Asn type II'  $\beta$ -hairpin that directly follows helix  $\alpha 6$  and precedes the omega loop (Figs 1a,b, 2). In OXA-10, the Asn side chain forms a hydrogen bond to the carbonyl oxygen of Gln 158 that lies in a  $3_{10}$ -helix directly following the omega loop. The N143S and G157D substitutions cannot be accommodated by the conformation of the omega loop observed in our structure. One can predict that the rearrangements necessitated by these mutations will affect the orientation of the adjacent active site residues (Trp 154 and Leu 155; Fig. 5a). OXA-14 and OXA-16 also contain the G157D mutation, with the latter having a second substitution, A124T. Ala 124 lies on helix  $\alpha 5$  and is tightly packed and buried within the molecule. Its side chain forms van der Waals contacts with the side chain of Trp 154, which would be altered upon substitution to the bulkier Val. In OXA-17, the substitution N73S (helix  $\alpha 3$ ) is observed. The side chain of Asn 73 forms van der Waals contacts with the side chains of Phe 69, Phe 120, Lys 70 and Trp 154 (Fig. 5a), which again would be altered upon substitution by the smaller Ser side chain. OXA-13, a narrow spectrum enzyme with a substrate preference for cefotaxime and aztreonam, also contains the N73S substitution. Interestingly, of the nine substitutions in OXA-13, only N73S is adjacent to the active site cleft. The majority of other changes are substitutions of negatively charged, solvated residues more than  $30 \text{ \AA}$  away from the active site (D55N, E229G and E259A). Other changes appear to be relatively conservative in terms of structure: the N-terminal G20S, T107S (the helix capping residue of helix  $\alpha 4$  that terminates with Ser 115) and Y174F.

**Implications for the mechanism of class D  $\beta$ -lactamases**  
Despite the many site-directed mutagenesis, crystallographic, inhibitory and kinetic investigations, there is still significant controversy regarding many of the mechanistic details for each of the class A, B and C  $\beta$ -lactamases<sup>3</sup>. In the serine hydrolase classes, perhaps the most experimentally supported proposals include the role of the serine nucleophile in acylation<sup>1,3</sup>, the role of Glu 166 as the general base in deacylation in the class A enzymes<sup>3</sup> (Fig. 5c), and an essential role of Tyr 150 in the class C enzymes (Fig. 5d)<sup>3,12,18,22</sup>. As comparisons of the active site region show that class D enzymes contain no counterparts to Glu 166 or Tyr 150, our structure would thus suggest that the catalytic mechanism by which class D enzymes hydrolyze  $\beta$ -lactam

antibiotics differs from the mechanism operating in the class A and C serine  $\beta$ -lactamases.

Based on our structure we can propose potential catalytic pathways for the hydrolysis of the  $\beta$ -lactam bond by class D  $\beta$ -lactamases. In agreement with earlier labeling studies<sup>23</sup>, the element 1 Ser 67 side chain hydroxyl would likely act as the nucleophile in the acylation step of the reaction, with electrostatic stabilization of the oxyanion transitional intermediate by the two main chain amides of the putative oxyanion hole (Ser 67 NH and Phe 208 NH; Fig. 5a). Our overlays of OXA-10 with the TEM-1/benzylpenicillin complex indicate that the hydroxyl of Ser 115 from element 2 is the only functional group within hydrogen bonding distance ( $\sim 2.9$  Å) of the nitrogen of the  $\beta$ -lactam bond to be cleaved (Fig. 5b). Thus, Ser 115 would appear to be a key intermediary in proton transfer from the Ser 67 hydroxyl to the nitrogen of the substrate. From our structure we can propose two possible ways the proton would be transferred to Ser 115 in OXA-10. Lys 70 N $\zeta$  would be optimally positioned to act as a general base. The buried, hydrophobic environment in which the Lys 70 side chain is situated in OXA-10 (Fig. 5a) would serve to depress its pK<sub>a</sub>, as would be required for such a role. Subsequently, the proton would be shuttled in a concerted manner to the hydroxyl of Ser 115 and then to the substrate leaving group (N4 in Fig. 5b). This transfer would be facilitated by the positive charges associated with Lys 70 and Lys 205 that would flank the Ser 115 hydroxyl in the tetrahedral intermediate I. Alternatively, we cannot rule out from our structure that acylation may occur *via* a direct transfer between the side chain hydroxyls of Ser 67 and Ser 115 (one molecule in the asymmetric unit has a hydrogen bond between these two residues, while the other does not).

A role for a general base Lys has been proposed for several bacterial serine hydrolases<sup>24–29</sup>, including the class A  $\beta$ -lactamases<sup>10,19</sup> (the latter with significant controversy<sup>3,30,31</sup>). Whatever the case may be in the class A enzymes, the environment of the element 1 Lys in the class D enzymes is substantially different, including the absence of a nearby negatively charged residue (Glu 166 in the class A enzymes) and of hydrogen bonds to the Asn in the active site element 2. This observation implies that the Lys residue (Lys 70) in OXA-10 may play a different role in catalysis.

How would deacylation of the acyl-enzyme intermediate occur in the class D  $\beta$ -lactamases? There is no counterpart to the conserved Glu 166 of the class A enzymes that has been suggested to act as the general base in deacylation by activating an appropriately positioned water to which it is hydrogen bonded (Fig. 5c)<sup>3</sup>. In the OXA-10 structure, a buried water is strongly hydrogen bonded to the N $\zeta$  of Lys 70 and the Ne of the conserved Trp 154 (Fig. 5a), a configuration that is unique to the class D enzymes. In terms of direction and distance, this water is a reasonable candidate for carrying out the nucleophilic attack on the carbonyl carbon of the acyl-enzyme intermediate, with general base assistance from Lys 70. The intimate connection between Ser 67, Lys 70 and WAT2 raises the possibility that deacylation is triggered by acylation. Such a tight coupling and possibly short lived acyl-enzyme intermediate may underlie the lower susceptibility of class D enzymes to existing mechanism-based inhibitors (which rely on forming inert esters) and may contribute to the broad substrate specificity of this class. It is compelling to note that directly adjacent to the water in the class D enzymes is the unique element 2 Val (Val 117). It may be that a hydrophobic residue is necessary at this position to provide the appropriate environment for catalysis (shielding the buried WAT2 and Lys N $\zeta$  from bulk solvent). This proposal may explain the deacylation deficiency of the related penicillin receptors BlaR<sup>20</sup>, MecR<sup>7</sup>, and the PBP's<sup>6</sup>, which all have a polar residue at this position in element 2 (Table 1, Fig. 2).

A classic feature of class D enzymes is the inhibition by chloride ions<sup>7,17</sup>. Full inhibition of OXA enzymes is observed at concentrations of 100 mM<sup>7,32,33</sup>. Preliminary evidence on OXA-10 crystals grown in the presence of 100 mM NaCl indicates that the largest difference in density occurs in the approximate position of WAT2. A chloride ion can be refined in this position (Fig. 3b), suggesting that this site may be the basis for inhibition by chloride in the class D enzymes (presumably displacing the proposed deacylating water and affecting the environment of Lys 70). The buried chloride has ligand distances of 2.8 Å and 3.2 Å to the N $\zeta$  and Ne1 of Lys 70 and Trp 154, respectively (a configuration similar to that observed in the 1.55 Å structure of the cardiotoxin from *Naja nigricollis*)<sup>34</sup>.

Finally, we cannot rule out alternative modes of deacylation, particularly in light of the sulfate ion adjacent to Ser 115 in the enzyme.

Table 3 Crystallographic data for OXA-10

Data collection								
Data set	$d_{\max}$ (Å) <sup>1</sup>	Reflections			I / $\sigma$ (I) (%)	$R_{\text{merge}}$ <sup>2</sup>	Sites <sup>3</sup>	
		Observed	Unique	% possible				
Native	2.0	139,455	37,894	93.4 (95.4) <sup>4</sup>	14.8 (10.1)	5.7 (14.7)	–	
K <sub>2</sub> PtCl <sub>4</sub>	2.2	73,653	27,871	90.7 (77.0)	21.9 (13.2)	4.1 (7.3)	2	
KAuCN	2.2	72,774	27,092	88.4 (88.0)	19.1 (11.7)	3.7 (8.9)	2	
NaCl	2.0	149,824	43,261	98.5 (97.1)	14.9 (7.0)	5.1 (14.5)	–	
Refinement statistics								
	Completeness of model			R-factor (%) <sup>5</sup>	$R_{\text{free}}$ (%) <sup>6</sup>	R.m.s. deviations		Overall B-factor (Å <sup>2</sup> )
	Residues	Atoms	Waters			Bonds (Å)	Angles (°)	
Native	492	3,888	293	19.0	21.4	0.006	1.3	19.6
NaCl	492	3,888	178	21.7	23.6	0.006	1.2	19.1

<sup>1</sup> $d_{\max}$  is the maximum resolution of measured X-ray intensities.

<sup>2</sup> $R_{\text{merge}} = \sum |I_{o,i} - I_{\text{ave},i}| / \sum I_{\text{ave},i}$ , where  $I_{\text{ave},i}$  is the average structure factor amplitude of reflection I and  $I_{o,i}$  represents the individual measurements of reflection I and its symmetry equivalent reflection.

<sup>3</sup>The overall figure of merit (FOM) for both derivatives including the anomalous signal was 0.47–2.2 Å resolution.

<sup>4</sup>The data collection statistics in brackets are the values for the highest resolution shell. The highest resolution shell for the derivative data sets was 2.20–2.28 Å, and was 2.00–2.07 Å for the native data set, and 1.97–2.07 Å for the NaCl data set.

<sup>5</sup>R-factor =  $\sum |F_o - F_c| / \sum F_o$  (on all data 2.0–20.0 Å)

<sup>6</sup> $R_{\text{free}} = \sum_{\text{hkl} \in T} (|F_o| - |F_c|)^2 / \sum_{\text{hkl} \in T} |F_o|^2$ , where  $\sum_{\text{hkl} \in T}$  are reflections belonging to a test set of 10% of the data, and  $F_o$  and  $F_c$  are the observed and calculated structure factors, respectively.

Although the direction would be less favorable, it may be that the presence of the sulfate in the active site of our structure displaces a potential nucleophilic water (with Ser 115 acting as general base).

### Methods

**Data collection.** OXA-10 was expressed and purified as described<sup>17</sup>. Crystals were grown by vapor diffusion using 1.8 M  $(\text{NH}_4)_2\text{SO}_4$ , 0.1 M 2-(N-Morpholino)ethanesulfonic acid (MES), 10 mM  $\text{CoCl}_2$  at pH 6.5. The crystals are in space group  $P2_12_12_1$  with unit cell dimensions of  $a = 48.4 \text{ \AA}$ ,  $b = 96.2 \text{ \AA}$ ,  $c = 125.7 \text{ \AA}$ . Data for  $\text{K}_2\text{PtCl}_4$  and  $\text{KAuCN}$  soaks (1 and 0.5 mM, respectively) were collected at 1.07225  $\text{\AA}$  and 1.04031  $\text{\AA}$ , respectively, at the Stanford Synchrotron Radiation Laboratory (SSRL), beamline 1-5, using an ADSC CCD detector, and processed with DENZO<sup>35</sup>.

**Phase determination and refinement.** Heavy atom sites and parameters were determined using SOLVE<sup>36</sup> and SHARP<sup>37</sup>. Solvent flattening was performed with SOLOMON<sup>37</sup>. Model building was performed with O<sup>38</sup> and refinement done using CNS<sup>39</sup> (Table 3).

**NaCl inhibition.** Crystals were grown in 1.6 M  $(\text{NH}_4)_2\text{SO}_4$ , 0.1 M Hepes, 0.1 M NaCl, 10 mM  $\text{CoCl}_2$  at pH 7.5. Crystals were isomorphous to those described above. Data were collected at the National Synchrotron Light Source (NSLS), beamline X12C, using a Brandeis Q4 CCD detector.

**Structural analysis.** Superpositions were performed with the algorithm LSQ within O<sup>38</sup> (cutoff 3.8  $\text{\AA}$ ). The dimer interface was analyzed using the protein-protein interaction server<sup>40</sup>. Hydrogen bond distances quoted in the text are an average of the two molecules in the asymmetric unit and are within 0.2  $\text{\AA}$  of each other.

**Analytical centrifugation.** Sedimentation equilibrium experiments were performed by centrifugation overnight at 18,000 r.p.m. using a Beckman Optima XA analytical centrifuge at 20 °C. The equilibrium between sedimentation and diffusion was followed by radial scanning of the 100  $\mu\text{l}$  tube at 280 nm until the equilibrium

condition was reached. The MW and partial specific volume of OXA-10 deduced from the amino acid sequence corresponded to 28.5 kDa and 0.740  $\text{cm}^3 \text{g}^{-1}$  (ref. 41). The absorbance profile at equilibrium was fitted to the MW distribution of the monomer and oligomers using Discreet<sup>42</sup>.

**Size exclusion chromatography.** Due to limitations of detection in the analytical ultracentrifugation method, at protein concentrations  $< 1 \mu\text{M}$  the apparent MW was estimated by size exclusion chromatography connected to a fluorescence detector. Measurements were performed using a Jasco HPLC connected to a Pharmacia Superdex 200 PC 3.2/30 gel filtration column. The column was equilibrated with buffer (three times the column volume) used for protein dilution in the enzyme assay. The flow rate was 0.1  $\text{ml min}^{-1}$  and 5  $\mu\text{l}$  of protein solution was injected. Elution of the protein was monitored by measuring its fluorescence (excitation at 280 nm, emission at 330 nm, FP920 intelligent Fluorescent detector, Jasco). Calibration of the column was performed using MW standards (Bio-Rad).

**Kinetic analysis.** OXA-10 (0.025  $\mu\text{M}$ ) was incubated for 20 min at room temperature in 20 mM Tris (adjusted to pH 7.0 with  $\text{H}_2\text{SO}_4$ ), and containing 0.3 M  $\text{K}_2\text{SO}_4$  and 0.5 mM metal salt (chloride or sulfate) when appropriate. The reaction was initiated by addition of 0.1 mM nitrocefin (final concentration). The change in absorbance was monitored at 490 nm using a Bio-Rad Model 3550 microtitreplate reader.

**Coordinates.** The coordinates have been deposited in the Protein Data Bank (accession code 1FOF).

### Acknowledgments

We thank the Medical Research Council of Canada (M.P. is a MRC fellow, N.C.J.S. is a MRC scholar), the Burroughs Wellcome Foundation (New Investigator Award to N.C.J.S.) and Hoffman-La Roche Pharmaceuticals (to F.D. and M.G.P.P.) for support. We thank H. Bellamy of beamline 1-5 at the SSRL for data collection access and R. Sweet for access to beamline X12C at the NSLS (Brookhaven National Laboratory).

Received 13 April, 2000; accepted 15 August, 2000.

1. Frère, J.M. Beta-lactamases and bacterial resistance to antibiotics. *Mol. Microbiol.* **16**, 385–395 (1995).
2. Joris, B., *et al.* Comparison of the sequences of class A beta-lactamases and of the secondary structure elements of penicillin-recognizing proteins. *Antimicrob. Agents Chemother.* **35**, 2294–2301 (1991).
3. Frère, J.M., Dubus, A., Galleni, M., Matagne, A. & Amicosante, G. Mechanistic diversity of beta-lactamases. *Biochem. Soc. Trans.* **27**, 58–63 (1999).
4. Bush, K. Metallo-beta-lactamases: a class apart. *Clin. Infect. Dis.* **27** (Suppl 1), S48–53 (1998).
5. Knox, J.R., Moews, P.C. & Frère, J.M. Molecular evolution of bacterial beta-lactam resistance. *Chem. Biol.* **3**, 937–947 (1996).
6. Gordon, E., Mouz, N., Duée, E. & Dideberg, O. The crystal structure of the penicillin-binding protein 2x from *Streptococcus pneumoniae* and its acyl-enzyme form: implication in drug resistance. *J. Mol. Biol.* **299**, 477–485 (2000).
7. Nass, T. & Nordmann, P. OXA-type beta-lactamases. *Curr. Pharm. Design* **5**, 865–879 (1999).
8. Mugnier, P., Casin, I., Bouthers, A.T. & Collatz, E. Novel OXA-10-derived extended-spectrum beta-lactamases selected *in vivo* or *in vitro*. *Antimicrob. Agents Chemother.* **42**, 3113–3116 (1998).
9. Bush, K. The evolution of beta-lactamases. *Ciba Found. Symp.* **207**, 152–163 (1997).
10. Strynadka, N.C.J., *et al.* Molecular structure of the acyl-enzyme intermediate in beta-lactam hydrolysis at 1.7 Å resolution. *Nature* **359**, 700–705 (1992).
11. Jelsch, C., Mourey, L., Masson, J.-M., & Samama, J.-P. Crystal structure of *Escherichia coli* TEM1 beta-lactamase at 1.8 Å resolution. *Proteins* **16**, 364–383 (1993).
12. Oefner, C. *et al.* Refined crystal structure of beta-lactamase from *Citrobacter freundii* indicates a mechanism for beta-lactam hydrolysis. *Nature* **343**, 284–289 (1990).
13. Monaghan, C., Holland, S. & Dale, J.W. The interaction of anthraquinone dyes with the plasmid-mediated OXA-2 beta-lactamase. *Biochem. J.* **205**, 413–417 (1982).
14. Sanschagrin, F., Couture, F. & Levesque, R.C. Primary structure of OXA-3 and phylogeny of oxacillin-hydrolyzing class D beta-lactamases. *Antimicrob. Agents Chemother.* **39**, 887–893 (1995).
15. Glusker, J.P. Structural aspects of metal liganding to functional groups in proteins. *Adv. Protein Chem.* **42**, 1–76 (1991).
16. Dale, J.W., & Smith, J.T. The dimeric nature of an R-factor mediated beta-lactamase. *Biochem. Biophys. Res. Commun.* **68**, 1000–1005 (1976).
17. Danel, F., Hall, L.M., Gur, D. & Livermore, D.M. OXA-16, a further extended-spectrum variant of OXA-10 beta-lactamase, from two *Pseudomonas aeruginosa* isolates. *Antimicrob. Agents Chemother.* **42**, 3117–3122 (1998).
18. Lobkovsky, E., *et al.* Crystallographic structure of a phosphonate derivative of the *Enterobacter cloacae* P99 cephalosporinase: mechanistic interpretation of a beta-lactamase transition-state analog. *Biochemistry* **33**, 6762–6772 (1994).
19. Maveyraud, L., Pratt, R.F. & Samama, J.P. Crystal structure of an acylation transition-state analog of the TEM-1 beta-lactamase. Mechanistic implications for class A beta-lactamases. *Biochemistry* **37**, 2622–2628 (1998).
20. Zhu, Y., *et al.* Structure, function, and fate of the BlaR signal transducer involved in induction of beta-lactamase in *Bacillus licheniformis*. *J. Bacteriol.* **174**, 6171–6178 (1992).
21. Jacob-Dubuisson, F., Lamotte-Brasseur, J., Dideberg, O., Joris, B. & Frere, J.M. Arginine 220 is a critical residue for the catalytic mechanism of the *Streptomyces albus* G beta-lactamase. *Protein Eng.* **4**, 811–819 (1991).
22. Dubus, A., Normark, S., Kania, K. & Page, M.G.P. The role of tyrosine 150 in catalysis of beta-lactam hydrolysis by AmpC beta-lactamase from *Escherichia coli* investigated by site-directed mutagenesis. *Biochemistry* **33**, 8577–8586 (1994).
23. Ledent, P., Raquet, X., Joris, B., Van Beeumen, J. & Frere J.M. A comparative study of class-D beta-lactamases. *Biochem. J.* **292**, 555–562 (1993).
24. Little, J.W., *et al.* Cleavage of LexA repressor. *Methods Enzymol.* **244**, 266–284 (1994).
25. Paetzel, M., *et al.* Use of site-directed chemical modification to study an essential lysine in *Escherichia coli* leader peptidase. *J. Biol. Chem.* **272**, 9994–10003 (1997).
26. Patricelli, M.P. & Cravatt, B.F. Fatty acid amide hydrolase competitively degrades bioactive amides and esters through a nonconventional catalytic mechanism. *Biochemistry* **38**, 14125–14130 (1999).
27. Birghan, C., Mundt, E. & Gorbalenya, A.E. A non-canonical ion proteinase lacking the ATPase domain employs the Ser-Lys catalytic dyad to exercise broad control over the life cycle of a double-stranded RNA virus. *EMBO J.* **19**, 114–123 (2000).
28. Keiler, K.C. & Sauer, R.T. Identification of active site residues of the Tsp protease. *J. Biol. Chem.* **270**, 28864–28868 (1995).
29. Haase, J. & Lanka, E. A specific protease encoded by the conjugative DNA transfer systems of IncP and Ti plasmids is essential for pilus synthesis. *J. Bacteriol.* **179**, 5728–5735 (1997).
30. Lietz, E.J., Truher, H., Kahn, D., Hokenson, M.J. & Fink, A.L. Lysine-73 is involved in the acylation and deacylation of beta-lactamase. *Biochemistry* **39**, 4971–4981 (2000).
31. Dambion, C., *et al.* The catalytic mechanism of beta-lactamases: NMR titration of an active-site lysine residue of the TEM-1 enzyme. *Proc. Natl. Acad. Sci. USA* **93**, 1747–1752 (1996).
32. Philippon, A.M., Paul G. & Jacoby, G.A. Properties of PSE-2 beta-lactamase and genetic basis for its production in *Pseudomonas aeruginosa*. *Antimicrob. Agents Chemother.* **24**, 362–369 (1983).
33. Bush, K., Jacoby G.A., Medeiros, A.A. A functional classification scheme for beta-lactamases and its correlation with molecular structure. *Antimicrob. Agents Chemother.* **39**, 1211–1233 (1995).
34. Bilwes, A., Rees, B., Moras, D., Menez, R., & Menez, A. X-ray structure at 1.55 Å of toxin gamma, a cardiotoxin from *Naja nigricollis* venom. Crystal packing reveals a model for insertion into membranes. *J. Mol. Biol.* **239**, 122–136 (1994).
35. Otwinowski, Z. In *Denzo* (eds, Sawyer, L., Isaacs, N. & Baily, S.) 56–62 (SERC Daresbury Laboratory, Warrington, UK; 1993).
36. Terwilliger, T.C. & Berendzen, J. Automated structure solution for MIR and MAD. *Acta Crystallogr. D* **55**, 849–861 (1999).
37. La Fortelle, E. & Bricogne, G. Maximum-likelihood heavy-atom parameter refinement in the MIR and MAD methods *Methods Enzymol.* **276**, 472–494 (1997).
38. Jones, T.A., Zou, J.-Y., Cowan, S.W. & Kjeldgaard, M. Improved methods for building protein models in electron density maps and the location of errors in these models. *Acta Crystallogr. A* **47**, 110–119 (1991).
39. Brünger, A.T. *et al.* Crystallography & NMR system: a new software suite for macromolecular structure determination. *Acta Crystallogr. D* **54**, 905–921 (1998).
40. Jones, S. & Thornton, J.M. Protein-protein interactions: a review of protein dimer structure. *Prog. Biophys. Mol. Biol.* **63**, 31–165 (1995).
41. Cohn, E.J. & Edsall, J.T. Density and apparent specific volume of proteins. In *Proteins, amino acids and peptides as ions and dipolar ions* (ed. E. J. Cohn), 370–381 (Reinhold, New York; 1943).
42. Schuck, P. Simultaneous radial and wavelength analysis with the Optima XL-A analytical ultracentrifuge. *Prog. Colloid Polymer Sci.* **94**, 1–13 (1994).
43. Kraulis, P. G. Molscript: a program to produce both detailed and schematic plots of protein structures. *J. Appl. Crystallog.* **24**, 946–950 (1991).
44. Nicholls, A., Sharp, K.A. & Honig, B. Protein folding and association: insights from the interfacial and thermodynamic properties of hydrocarbons. *Proteins* **11**, 281–296 (1991).
45. Couture, F., Lachapelle, J. & Levesque, R.C. Phylogeny of LCR-1 and OXA-5 with class A and class D beta-lactamases. *Mol. Microbiol.* **6**, 1693–1705 (1992).
46. Thompson, J.D., Higgins, D.G. & Gibson, T.J. CLUSTAL W: improving the sensitivity of progressive multiple sequence alignment through sequence weighting, positions-specific gap penalties and weight matrix choice. *Nucleic Acids Res.* **22**, 4673–4680 (1994).